ORIGINAL ARTICLE

JBMR®

Prostate Cancer Cells Preferentially Home to Osteoblast-rich Areas in the Early Stages of Bone Metastasis: Evidence From In Vivo Models

Ning Wang,[1] Freyja E Docherty,[1] Hannah K Brown,[1] Kimberley J Reeves,[2] Anne CM Fowles,[1] Penelope D Ottewell,[3] T Neil Dear,[4] Ingunn Holen,[3] Peter I Croucher,[5] and Colby L Eaton[1]

[1]The Mellanby Centre for Bone Research, Department of Human Metabolism, The University of Sheffield, Sheffield, UK
[2]Break Through Breast Cancer Research Unit, Paterson Institute for Cancer Research Manchester, UK
[3]Department of Oncology, The University of Sheffield, Sheffield, UK
[4]South Australian Health and Medical Research Institute, Adelaide, South Australia, Australia
[5]Garvan Institute of Medical Research, Sydney, New South Wales, Australia

ABSTRACT

It has been suggested that metastasis-initiating cells gain a foothold in bone by homing to a metastastatic microenvironment (or "niche"). Whereas the precise nature of this niche remains to be established, it is likely to contain bone cell populations including osteoblasts and osteoclasts. In the mouse tibia, the distribution of osteoblasts on endocortical bone surfaces is non-uniform, and we hypothesize that studying co-localization of individual tumor cells with resident cell populations will reveal the identity of critical cellular components of the niche. In this study, we have mapped the distribution of three human prostate cancer cell lines (PC3-NW1, LN-CaP, and C4 2B4) colonizing the tibiae of athymic mice following intracardiac injection and evaluated their interaction with potential metastatic niches. Prostate cancer cells labeled with the fluorescent cell membrane dye (Vybrant DiD) were found by two-photon microscopy to be engrafted in the tibiae in close proximity (~40 μm) to bone surfaces and 70% more cancer cells were detected in the lateral compared to the medial endocortical bone regions. This was associated with a 5-fold higher number of osteoblasts and 7-fold higher bone formation rate on the lateral endocortical bone surface compared to the medial side. By disrupting cellular interactions mediated by the chemokine (C-X-C motif) receptor 4 (CXCR4)/chemokine ligand 12 (CXCL12) axis with the CXCR4 inhibitor AMD3100, the preferential homing pattern of prostate cancer cells to osteoblast-rich bone surfaces was disrupted. In this study, we map the location of prostate cancer cells that home to endocortical regions in bone and our data demonstrate that homing of prostate cancer cells is associated with the presence and activity of osteoblast lineage cells, and suggest that therapies targeting osteoblast niches should be considered to prevent development of incurable prostate cancer bone metastases. © 2014 American Society for Bone and Mineral Research.

KEY WORDS: PROSTATE CANCER; BONE METASTASIS; OSTEOBLAST NICHE; TWO-PHOTON MICROSCOPY

Introduction

Prostate cancer is the second most commonly diagnosed cancer in men and the sixth leading cause of cancer death globally.[1] In economically developed countries, prostate cancer is second only to lung cancer as the most frequent cancer and has the third highest mortality rate.[1] Although patients with prostate cancer have a relatively slowly growing primary tumor, which can be eradicated by current treatments, it is the presence of metastases that results in significant disease morbidity and mortality. Around 90% patients with metastases have incurable bone metastases,[2] which are often associated with intractable bone pain, pathological fractures, and decreased quality of life. Our understanding of the specific mechanism responsible for development of prostate cancer bone metastasis remains incomplete. As the preferred metastatic site, bone provides a supportive a microenvironment or "niche" where prostate cancer cells can reside, survive, and eventually grow in accordance with Paget's century old "seed and soil" hypothesis.[3,4] Recent studies using murine models and xenografted human prostate cancer cell lines have shown that prostate cancer cells target haemopoietic stem cell (HSC) niches and compete with HSCs to facilitate the establishment of bone metastases.[5,6] The mobilization and proliferation of HSCs is suggested to be supported by the vascular niche, while the endosteal niche (including osteoblasts) maintains HSCs as a quiescent or reserve population.[6–8] Osteoblasts are suggested to fulfill this task via interacting with HSCs through sets of surface molecules,

Received in original form April 17, 2014; revised form June 6, 2014; accepted June 13, 2014. Accepted manuscript online June 23, 2014.
Address correspondence to: Colby L Eaton, PhD, The Mellanby Centre for Bone Research, Department of Human Metabolism, The University of Sheffield, Beech Hill Road, Sheffield, S10 2RX UK. E-mail: c.l.eaton@sheffield.ac.uk

Journal of Bone and Mineral Research, Vol. 29, No. 12, December 2014, pp 2688–2696
DOI: 10.1002/jbmr.2300

including Tie2/Angiopoietin-1 (Ang-1), Jagged1/Notch1, N-Cadherin, and CXCR4/CXCL12.[5,9–15] In the case of the latter, CXCR4 is expressed by prostate cancer cells and CXCL12 by osteoblasts. This CXCR4/CXCL12 axis is considered to be a key component in the homing, adhesion, and survival of prostate cancer cells in bone.[5,16–21]

Given that the distribution of the osteoblast lineage cells is not uniform within the bone, it is likely that HSC niches are not uniformly located across the bone marrow. In the mouse tibia, this topographical variation is more obvious on the endocortical surfaces than in the trabecular regions. This is because of skeletal response to mechanical loading and the consequent nature of bone resorption and formation required for bone modeling, in which osteoblastic bone formation predominantly occurs on lateral endocortical bone surfaces whereas osteoclastic resorption is found predominantly on medial endocortical bone surfaces.[22] In this study, we hypothesized that the prostate cancer cells homing to the bone marrow should have a similar spatial distribution pattern as the HSC osteoblast niches. We performed a series of experiments to test this hypothesis by mapping the early homing of human prostate cancer cells into the mouse tibia in a xenograph model, using a unique combination of two-photon microscopy and bone histomorphometry. We also tested whether the distribution pattern of prostate cancer cells in bone could be altered by disrupting the CXCR4/CXCL12 axis involved in cancer cell homing. These studies provide the first direct evidence that during the very early stages of bone metastasis, cancer cells locate to the areas of bone with the highest number of osteoblast lineage cells and that these cells play a significant role in establishing a foothold for prostate cancer cells metastases in bone, possibly via CXCR4/CXCL12 axis.

Materials and Methods

Mice

Six-week-old male BALB/cAnNCrl immunocompromised (athymic nude) mice (Charles River, Kent, UK) were used as a model to examine prostate cancer cells distribution in bone. Transgenic mice engineered to express GFP under the control of type 1 collagen promoter (pOBCol2.3GFPemd)[23] kindly provided by Prof. David Rowe, University of Connecticut, Storrs, CT, USA) were backcrossed so that the transgene was congenic on a BALB/cAnNCrl Foxn1$^{nu/nu}$ background thus generating immunocompromised mice expressing GFPemd in cells of osteoblast lineage (C.BALB/cAnNCrl-Tg(Col1a1-GFP)Row Foxn1$^{nu/nu}$. These mice were hereafter referred to as Col-GFP nude mice and were used as a model to investigate the link between disseminated cancer cells and resident osteoblasts. Mice were housed in a controlled environment in Optimice cages (Animal Care Systems, Centennial, CO, USA) with a 12 hr light/dark cycle at 22°C with *ad libitum* 2018 Teklad Global 18% protein rodent diet containing 1.01% calcium (Harlan Laboratories, Derby, UK) and water. All procedures complied with the UK Animals (Scientific Procedures) Act 1986 and were reviewed and approved by the local Research Ethics Committees of the University of Sheffield under Home Office project license 40/3462 (Sheffield, UK).

Cell lines

PC3-NW1 is a substrain of the commonly used human prostate cancer cell line PC3 (ATCC, Middlesex, UK), which was stably transfected with a firefly luciferase gene *luc2* (pGL4.51 [luc2/CMV/Neo] vector, Promega, Southampton, UK) using a Gene Pulser electroporator (Bio-Rad Laboratories Ltd, Hemel Hempstead, UK). Two other human prostate cancer cell lines, C4 2B4 and LN-CaP were also purchased from ATCC. All cell lines were maintained in Dulbecco's modified Eagle medium (DMEM) with 4.5 g/L glucose and sodium pyruvate (Gibco, Life Technologies, Paisley, UK), supplemented with 100 Units/ml penicillin and 100 μg/ml streptomycin (Gibco) and 10% fetal calf serum (FCS) (Sigma Aldrich Co Ltd, Poole, UK).

Intracardiac inoculation of prostate cancer cells

Prostate cancer cells were initially labeled with 5 μM lipophilic carbocyanine dye Vybrant DiD (Life Technologies, Paisley, UK) according to the manufacturer's manual. A single-cell suspension of 1×10^5 DiD labeled cancer cells/100 μL PBS was injected into the left cardiac ventricle (i.c injection) of 6-week-old male Balb/c nude mice. Cohorts of animals (minimum six in each group) were euthanized at different time points (1 day, 7 days, 3 and 6 weeks post tumor cell injection) and the presence of DiD labeled cancer cells were mapped in the tibiae by two-photon microscopy. Bone histomorphometry was used to determine the topography of resident cell populations within the tibiae.

Two-photon microscopy

Dissected tibiae were embedded in Cryo-M-Bed embedding compound (Bright Instrument Co. Ltd, Huntingdon, UK) after being snap-frozen in liquid nitrogen and were trimmed longitudinally to expose the bone marrow using a Bright OTF Cryostat with a 3020 microtome (Bright Instrument). A Zeiss LSM510 NLO upright two-photon microscope (Carl Zeiss Microscopy Ltd, Cambridge, UK) was then used to image a stack area of 2104 μm × 2525 μm below the growth plate, 100 μm in depth. The image was then reconstructed with the LSM software 4.2 (Carl Zeiss Microscopy). A 633 nm HeNe laser was used to detect DiD labeled cells, while bone and GFP expressing osteoblasts were detected using the 900 nm Chameleon multiphoton laser (Coherent, Santa Clara, CA, USA).

In the dynamic bone histomorphometry studies, alizarin complexone labels were detected using a 543 nm laser while bone and calcein labels were detected using the 900 nm two-photon laser. Within 300 μm of endocortical bone surfaces (one third of the cross-sectional diameter of bone marrow cavity in tibial metaphysis region), the number of cancer cells, the intensity of DiD labeling of cancer cells, and minimal distance from centroid of these cells to the lateral and medial endocortical bone surfaces, were then analyzed using the Volocity 3D Image Analysis software 6.01 (PerkinElmer, Cambridge, UK).

Bone histomorphometry

The tibiae were dissected and fixed in 10% buffered formaldehyde, decalcified in 14.3% EDTA, and then embedded in paraffin wax so that a complete longitudinal section could be cut. Sections were cut longitudinally at 3 μm thickness and tartrate-resistant acid phosphatase (TRAP) stained as described previously.[24] The number of osteoblasts (N.Ob/B.Pm), osteoblast surface (Ob.Pm/B.Pm), the number of osteoclasts (N.Oc/B.Pm), and the osteoclast surface (Oc.Pm/B.Pm) were determined on a 1.5 mm length of lateral and medial endocortical surfaces, using a DMRB microscope (Leica Microsystems, Wetzlar, Germany). All histomorphometric parameters were based on the report of the ASBMR Histomorphometry Nomenclature Committtee[25] and

were obtained using the Osteomeasure bone histomorphometry software (OsteoMetrics, Inc., Decatur, GA, USA).

Dynamic bone histomorphometry

To determine the different bone remodeling activities on lateral and medial endocortical bone surfaces, mice were injected intraperitoneally with Alizarin complexone (20 mg/kg, Sigma-Aldrich) on day 0 and calcein (30 mg/kg, Sigma-Aldrich) on day 6, post cancer cell injection. The mice were euthanized 7 days post tumor injection and the tibiae were then dissected and fixed in 70% ethanol, followed by embedding into LR White resin (Taab Laboratory Equipment Ltd, Reading, Berkshire, UK). Sections were cut at 10 μm using a Leica Microsystems Microtome. Mineral apposition rates (MAR), mineralizing surface (MS), and the bone formation rates (BFR/BS) were obtained using a BioQuant Osteo image analysis system (BIOQUANT, Nashville, TN, USA).

Mobilization of bone homing cancer cells by a CXCR4 inhibitor

Six-week-old male Balb/c nude mice were injected (i.c.) with 1×10^5 DiD labeled PC3-NW1 cells. Seven days after cancer cell injection, animals were subject to 5 days of treatment with the CXCR4 inhibitor AMD3100 (marketed as Plerixafor) (5 mg/kg, daily intraperitoneal injection in 100 μL PBS) (Sigma Aldrich) or PBS control. Animals were then euthanized and the distributions of DiD labeled PC3 NW1 cells were examined in the tibiae by two-photon microscopy ex vivo and analyzed with the Volocity 3D Image analysis software.

Statistical analysis

All data are expressed as mean ± SEM. Statistical significance was tested for two-tailed paired or unpaired *t* test as appropriate with Prism 5 software (GraphPad, La Jolla, CA, USA): $p < 0.05$ was considered to be significant ($^{*}p < 0.05$, $^{**}p < 0.01$, $^{***}p < 0.001$, $^{****}p < 0.0001$).

Results

Spatial distribution of PC3-NW1 prostate cancer cells homing to mouse tibiae

Seven days after injection of DiD labeled PC3-NW1 cells, mice were euthanized, and tibiae were collected and processed for two-photon microscopy. The DiD labeled PC3-NW1 cells were observed in close proximity to bone, including both lateral and medial endocortical bone surfaces within the bone marrow (Fig. 1*A*). Initial evaluation of microscope images from 11 separate mice showed a higher frequency of DiD signals detected in close proximity to lateral endocortical surfaces (Fig. 1*B*, *C*). DiD labeled PC3-NW1 cancer cells were found to be located within 300 μm from endocortical surface. Significantly higher numbers of cancer cells per mm bone surface were observed on the lateral compared to the medial endocortical surfaces (11.74 ± 3.68 versus 4.65 ± 0.98 mm^{-1}, $p = 0.033$) (Fig. 1*C*). There was no significant difference in the minimum distance of tumor cells to the nearest bone surfaces between the lateral and medial endocortical bone surfaces (35.31 ± 3.70 versus 28.26 ± 6.85 μm, $p = 0.173$) (Fig. 1*D*). The preferential location of prostate cancer cells to lateral over medial endocortical surfaces was maintained at later time points including at 3 weeks (6.50 ± 1.75 versus 2.18 ± 0.56 mm^{-1}, $p = 0.029$) and at 6 weeks (3.80 ± 1.18 versus 0.56 ± 0.19 mm^{-1}, $p = 0.017$) after cancer cell injection. However, at 24 hours there was no difference in tumor cell numbers between the two surfaces (7.08 ± 1.48 versus 4.46 ± 0.68 mm^{-1}, $p = 0.098$) (Fig. 1*E*). The intensity of DiD staining of prostate cancer cells reach a peak value on day 7 and then started to slowly decline (Fig. 1*F*), indicating the homed cancer cells did not start growth within the first 7 days after injection. These data suggest that there is a particular distribution pattern of prostate cancer cells localized in bone, including close proximity to bone surfaces and preferential homing to the lateral endocortical compared to medial surfaces.

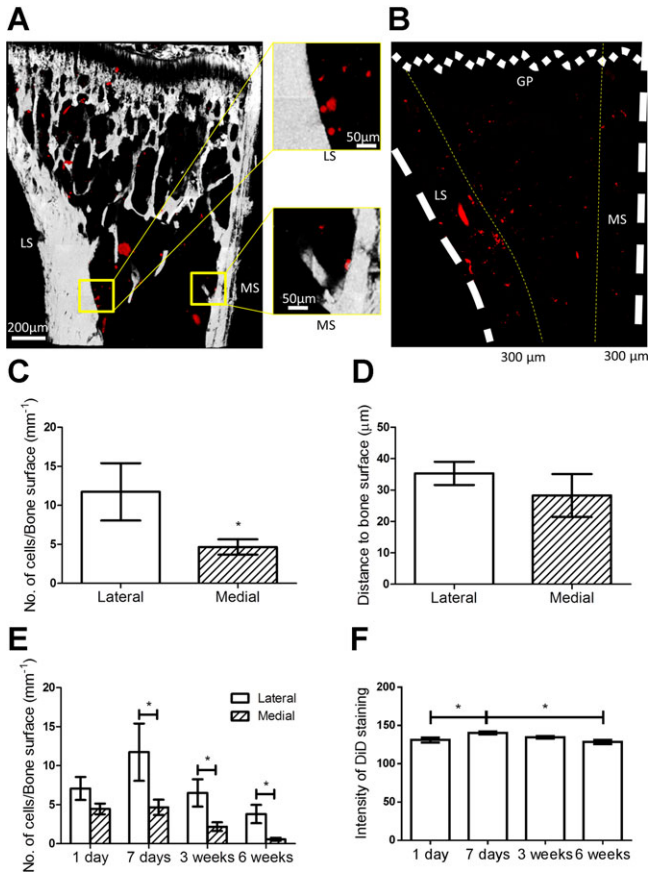

Fig. 1. Preferential homing of prostate cancer cells to lateral endocortical bone surfaces in the tibia. *(A)* Vybrant DiD labeled PC3-NW1 cells were injected i.c. into 6-week-old BALB/c nude male mice and visualized in tibiae 7 days postinjection using two-photon microscopy (MP). LS = lateral side, MS = medial side. *(B)* Cartoon generated by superimposing scans from 11 mice showed higher frequency of DiD signals in close proximity to lateral endocortical surfaces. DiD labeled PC3-NW1 cells detected within 300 μm from endocortical surface were quantified using the Volocity 3D Image analysis software. *(C)* The number of cancer cells homing to the lateral side bone surfaces and *(D)* the distance from these cancer cells to bone surfaces were compared with those homing to the medial surfaces, $n = 11$, $^{*}p < 0.05$, paired *t* test. *(E)* Detection of DiD positive tumor cells in bone and *(F)* the intensity of DiD fluorescence after 1 day and 7 days, 3 and 6 weeks postinjection, $n > 6$, $^{*}p < 0.05$, paired and unpaired *t* test, respectively.

The preferential homing of other prostate cancer cell lines to lateral endocortical surfaces

In order to investigate whether the homing pattern observed was independent of prostate cancer cell type, DiD labeled C4 2B4 and LN-CaP prostate cancer cells were also injected i.c. into 6-week-old Balb/C nude male mice. DiD labeled cells were found in tibiae of mice in both experiments and the distribution of these cancer cells in tibial endocortical bone regions were determined 7 days postinjection using a two-photon microscope (Fig. 2*A*, *D*). These analyses (Volocity 3D Image analysis software) showed that there was a 73% increase in number of C4 2B4 cells homing to the lateral endocortical surface compared to the medial side (11.62 ± 2.24 versus 6.73 ± 1.46 mm^{-1}, $p = 0.024$) (Fig. 2*B*), but no significant difference in the minimum distance from cancer cells to the lateral or medial surfaces were seen (42.15 ± 6.43 versus 49.96 ± 12.13 μm, $p = 0.529$) (Fig. 2*C*). LN-CaP prostate cancer cells also showed a similar trend with 114% more cells homing to the lateral compared to medial side (7.17 ± 1.50 versus 3.35 ± 0.72 mm^{-1}, $p = 0.013$) (Fig. 2*E*). There was no statistically significant difference in the minimum distance from cancer cells to the nearest bone surfaces (lateral 35.53 ± 5.65 versus medial 59.04 ± 9.98 μm, $p = 0.090$) (Fig. 2*F*). Taken together, these data support that the lateral versus medial pattern of cancer cell distribution in bone is not a unique phenomenon for PC3-NW1 cells, but also applies to other prostate cancer cell lines including LN-CaP and C4 2B4.

Bone formation differs between lateral and medial endocortical bone surfaces

To examine the different bone formation activities on lateral and medial endocortical bone surfaces, mice were injected with Alizarin Complexone on day 0 and calcein on day 6 after cancer cell injection. Two distinctive alizarin and calcein labels on the proximal endocortical surfaces of tibiae were visualized using two-photon microscopy (Fig. 3*A*). The double labels were imaged and quantified using the BioQuant Osteo image analysis system to calculate the bone formation related parameters including MS, MAR, and the BFR/BS (Fig. 3*B*). All these parameters showed

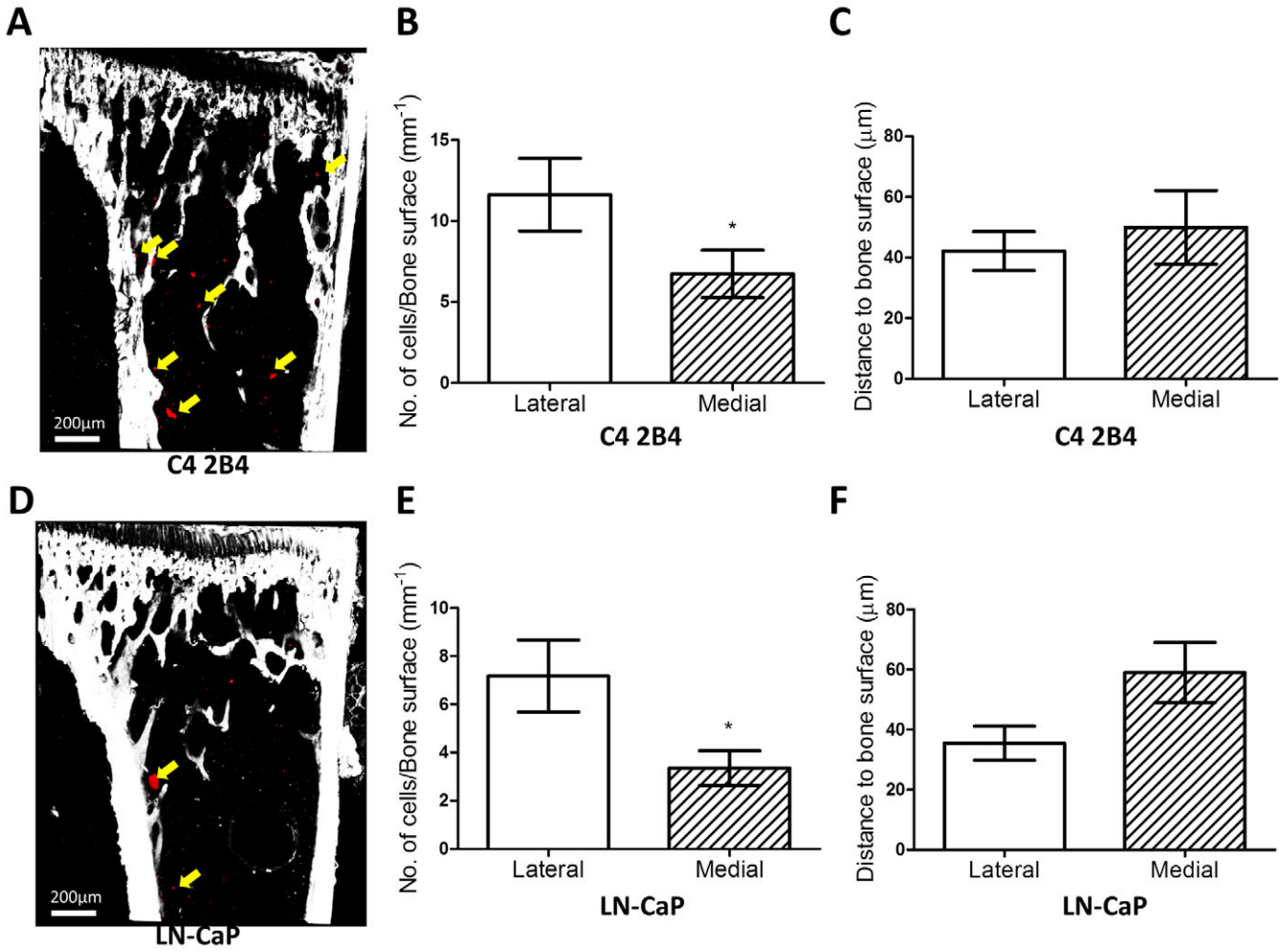

Fig. 2. Homing of C4 2B4 and LN-CaP prostate cancer cells to bone. Vybrant DiD labeled C4 2B4 and LN-CaP prostate cancer cells were injected i.c. into 6-week-old BALB/c nude male mice. *(A, D)* The location of cancer cells (yellow arrows) was visualized in tibiae 7 days postinjection using two-photon microscopy. *(B, E)* The number of cancer cells homing to the lateral side bone surfaces and *(C, F)* the distance from these cancer cells to bone surfaces compared with those homing to the medial surfaces, $n = 8$, $^*p < 0.05$, paired *t* test.

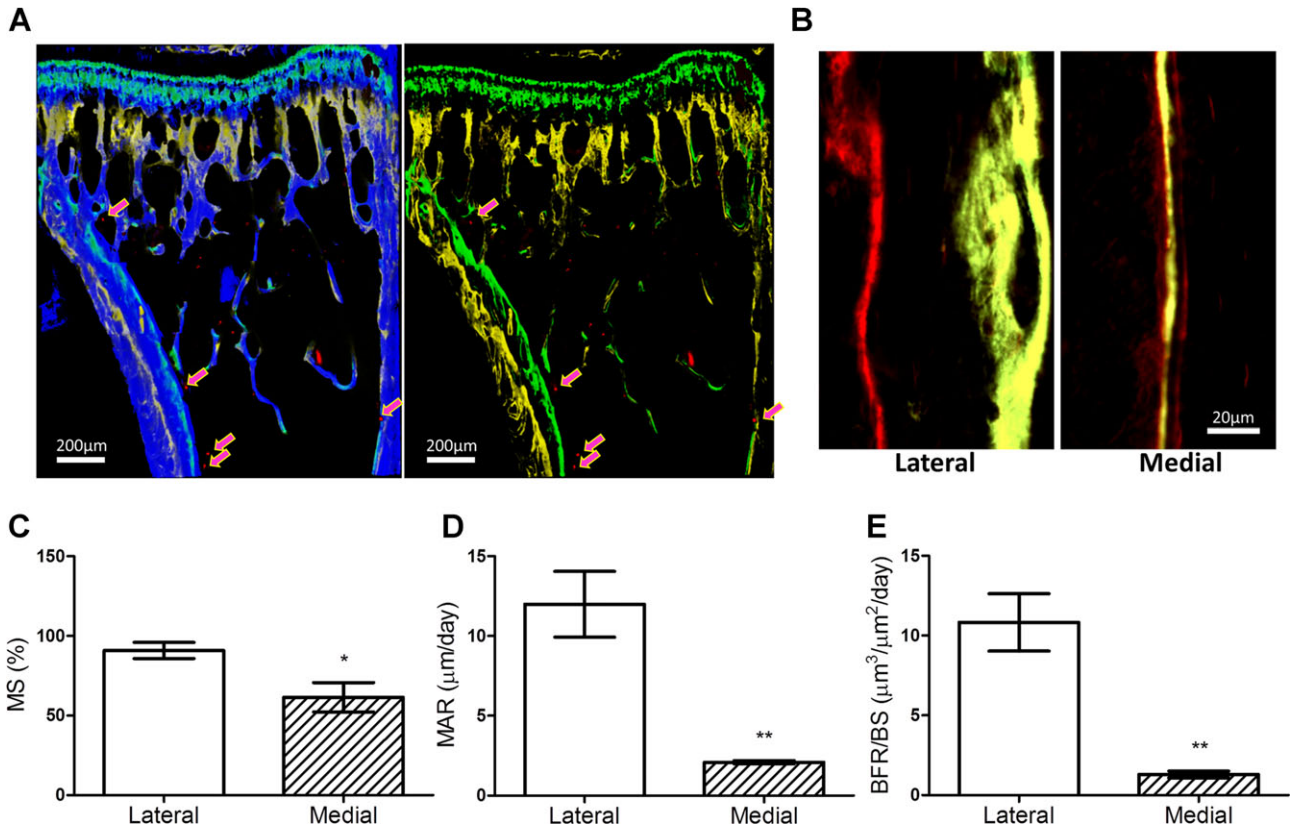

Fig. 3. Bone formation activities on lateral and medial endocortical bone surfaces. Vybrant DiD labeled PC3-NW1 cells were injected i.c. into 6-week-old BALB/c nude male mice. Alizarin Complexone and calcein were injected intraperitoneally on day 0 and day 6, respectively, to examine the bone formation activities. *(A)* Double labeling (alizarin in yellow and calcein in green) of mouse tibia with DiD labeled PC3-NW1 cells (pink arrows) homing to endocortical bone surface (bone in blue) were visualized using two-photon microscopy, 7 days after tumor cell injection. *(B)* The double labeling visualizing newly formed bone were then imaged and scored using the BioQuant Imaging system. *(C)* The mineralized surface (MS), *(D)* mineral apposition rate (MAR), and *(E)* bone formation rate (BFR/BS) were scored and compared between the lateral and medial endocortical bone. $n = 6$, $^{*}p < 0.05$, $^{**}p < 0.01$, paired t test.

significantly higher values on the lateral compared to the medial endocortical surfaces, including 48% higher MS (90.86 ± 5.06 versus $61.47 \pm 9.20\%$, $p = 0.023$), 475% higher MAR (11.99 ± 2.06 versus 2.09 ± 0.10, $p = 0.004$), and 739% higher BFR/BS (10.83 ± 1.80 versus 1.29 ± 0.21, $p = 0.002$) (Fig. 3*C–E*). Therefore, the areas of bone where prostate cancer cells preferentially home also undergo higher rates of bone formation, indicating a role for the osteoblast.

Differential bone cells distribution between lateral and medial endocortical surfaces

To study the spatial relationship between osteoblast and prostate cancer cells, immunocompromised mice expressing GFPemd in cells of osteoblast lineage were used. DiD labeled PC3-NW1 cells were injected via the intracardiac route and the presence of tumor cells in the tibiae were analyzed 7 days later. Two-photon imaging showed that higher number of cancer cells had homed to the GFP expressing, osteoblast-rich, lateral endocortical compared to medial regions and some cancer cells was found in direct contact with osteoblasts (Fig. 4*A*). The tibiae were sectioned and TRAP stained to facilitate imaging and scoring of bone cells on endocortical bone surfaces (Fig. 4*B*). Histomorphometric analysis of the cellular compartment of different bone regions showed that there was a 5-fold increase in number of osteoblasts on the lateral compared to the medial surface (N. Ob/B.Pm, 56.14 ± 6.46 versus 9.84 ± 3.72 mm^{-1}, $p < 0.001$) (Fig. 4*C*), with osteoblasts covering 4-fold more bone surface (Ob.Pm/B.Pm, 0.73 ± 0.08 versus 0.15 ± 0.05, $p < 0.001$) (Fig. 4*D*). The osteoclasts' parameters showed an opposite trend, with the lateral endocortical bone surface having fewer osteoclasts (N.Oc/B.Pm 0.23 ± 0.15 versus 1.42 ± 0.52 mm^{-1}, $p = 0.072$) (Fig. 4*E*) and fewer osteoclast-covered bone surfaces (Oc.Pm/B.Pm 0.005 ± 0.003 versus 0.049 ± 0.018, $p = 0.056$) (Fig. 4*F*).

Effects of disruption of the CXCR4/CXCL12 axis on cancer cell distribution

Disruption of the CXCR4/CXCL12 axis with CXCR4 inhibitor (AMD3100) has been shown to mobilize prostate cancer cells that had homed to the bone microenvironment in a xenograft model.[5] To determine whether disruption of the CXCR4/CXCL12 axis would change the spatial distribution of cancer cells in bone in our models, animals received five daily injections of AMD3100, starting 7 days after cancer cell injection (Fig. 5*A*). Two-photon

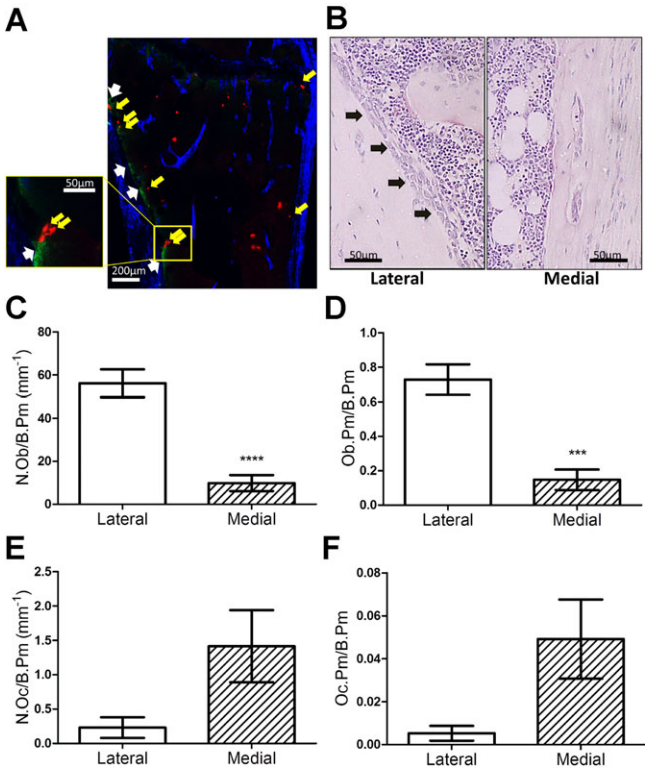

Fig. 4. The distribution of bone cells on endocortical bone surfaces. The Vybrant DiD labeled PC3-NW1 cells were injected i.c. into male 6-week-old pOBCol2.3GFPemdBALB/c nude (Col-GFP) mice. *(A)* Seven days postinjection, two-photon imaging was used to establish the distribution pattern of DiD labeled PC3-NW1 cells (yellow arrows) homing to the metaphysis. Osteoblasts express GFP are in green (white arrows) and bone is visualized in blue. *(B)* Bright field microscope images of a representative TRAP-stained longitudinal tibia section showed abundant osteoblasts (black arrows) on the lateral endocortical bone surface. Osteomeasure quantification confirmed the lateral surface had *(C)* more osteoblasts (N.Ob/B.Pm) and *(D)* higher osteoblast coverage (Ob.Pm/B.Pm), while the medial surface had *(E)* more osteoclasts (N.Oc/B.Pm) and *(F)* higher osteoclast coverage (Oc.Pm/B.Pm), $n = 7$, compared to the medial surface $^{***}p < 0.001$, $^{****}p < 0.0001$, paired *t* test.

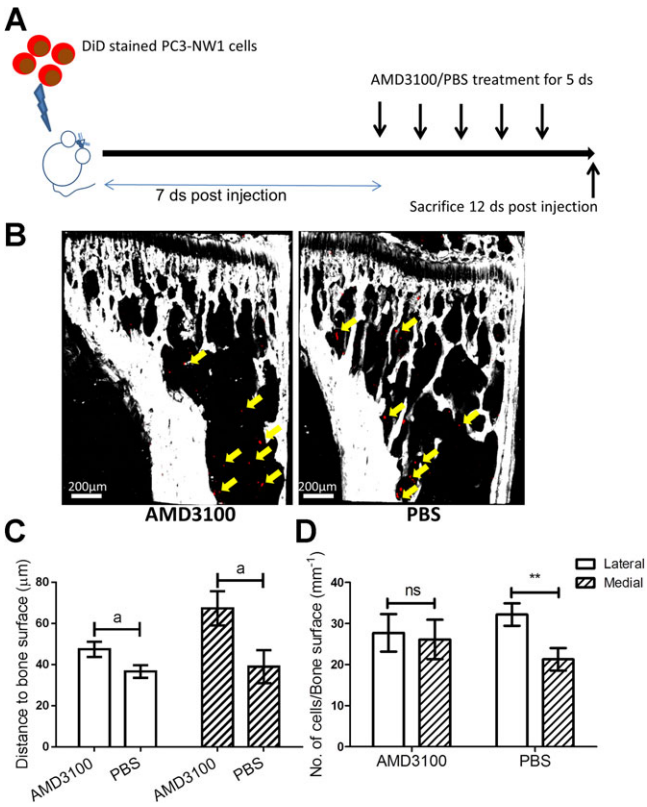

Fig. 5. Distribution of cancer cells after disruption of CXCR4/CXCL12 axis. *(A)* Schematic outline of the procedure used to evaluate the effects of the CXCR4 inhibitor AMD3100 on the distribution of PC3-NW1 cells in vivo. *(B)* Two-photon microscope analysis showed there were DiD labeled PC3-NW1 cells (yellow arrows) present in bone marrow after 5 days of treatment with AMD3100. Volocity 3D Image analysis showed *(C)* the alteration of minimum distance from cancer cells to different endocortical bone surfaces and *(D)* the changes of DiD labeled PC3-NW1 cells preferentially homing to lateral endocortical bone surfaces in AMD3100 treated group compared to vehicle group. $n = 7$, $^{*}p < 0.05$, $^{**}p < 0.01$, paired *t* test; $^{a}p < 0.05$, unpaired *t* test.

microscope imaging showed the presence of DiD labeled PC3-NW1 cells in both the AMD3100 treated and the vehicle group (Fig. 5*B*). AMD3100 treatment significantly increased the minimum distance from cancer cells to both lateral (47.49 ± 3.69 versus 35.94 ± 3.52 μm, $p = 0.047$, unpaired *t* test) and medial (67.43 ± 8.33 versus 39.04 ± 8.02 μm, $p = 0.033$, unpaired *t* test) bone surfaces (Fig. 5*C*). The AMD3100 treatment also led to changes in the distribution of homed cancer cells. There was no longer a significant difference in the number of cancer cells that were located at the lateral endocortical surface compared to the medial side (27.72 ± 4.57 versus 26.13 ± 4.79 mm^{-1}, $p = 0.722$). In contrast, in the vehicle group, there was still 51% more DiD labeled cancer cells detected at the lateral side compared to the medial side (31.18 ± 2.74 versus 21.29 ± 2.73 mm^{-1}, $p = 0.008$) (Fig. 5*D*). These data suggested that the spatial distribution of prostate cancer cells in bone could be altered as a result of disruption of CXCR4/CXCL12 axis.

Discussion

Prostate cancer cells have been shown to home to the endosteal niche of the metaphysis region of the long bones prior to the development of bone metastases.[5,6] Because the distribution of osteoblast lineage cells is not uniform within the metaphysis regions, we hypothesized that the spatial distribution of prostate cancer cells homed to bone should follow a pattern that correlates with the distribution of niches, and that the location of cancer cells would be altered if the linkage to their bone niches were disrupted.

In this study, we used three prostate cancer cell lines as metastatic models to investigate the bone homing process after i.c. inoculation into immunocompromised mice. Using the fluorescent dye DiD as a marker to monitor the proliferation of prostate cancer cells in vivo,[26] cancer cells were shown to maintain DiD fluorescence at a high level up to 7 days after injection, suggesting that no significant proliferation had started by this time point. This result demonstrated

that inoculated cancer cells were still involved in the process of homing rather than growth within this period, which is consistent with previous studies using different models.[27,28] Our results indicated that prostate cancer cells preferentially home to the osteoblast-rich lateral endocortical bone surface of the tibiae where bone formation rates are higher, rather than to the medial side with fewer osteoblasts and lower bone formation rates. These observations provided further evidence for interactions between cells of osteoblast lineage and prostate cancer cells that are homing to the bone marrow.

Two-photon microscopy and Volocity 3D image analysis were used to map the specific location of cancer cells that had homed to bone marrow. For all three prostate cell lines used in this study, individual cancer cells were detected in close proximity to bone surfaces 7 days postinjection, especially on the lateral side where the distance from a cancer cell to the closest bone surface was $\leq$40 μm. This finding suggests that prostate cancer cells home to regions where they have close access to the bone matrix and/or bone surface cells. The mineralized bone matrix is a main reservoir for growth factors that can affect the behaviors of cancer cells such as tumor growth factor-β (TGF-β) and bone morphogenic protein 7 (BMP-7).[29–31] These growth factors are released in areas of high bone turnover and could be one of the possible reasons why prostate cancer cells are attracted to home closely to bone surfaces, but it is a strong possibility that the presence of cells of the osteoblast lineages is the attraction for tumor cells. As the diameter of a typical osteoblast is between 15 and 30 μm,[32] cancer cells were located less than 40 μm away from the closest bone surface, suggesting that they are around one to two cell diameters away from the bone. It is likely that the cells between the bone surface and the cancer cell are of osteoblast lineage, as has been shown in a previous study.[5] Indeed, further investigation of the spatial distribution of prostate cancer cells within bone marrow showed that there was at least 70% higher frequency of cancer cells present on the lateral endocortical bone surface, where there are more resident osteoblasts and higher bone formation rates, compared to those on the medial endocortical surface. These findings indicate that the homing of cancer cells is correlated with the distribution of osteoblast-rich niches. Using the Col-GFP mice as model, our data further confirmed these findings and showed higher numbers of prostate cancer cells located near GFP-rich lateral endocortical regions and in some cases in direct contact with GFP expressing osteoblasts. While these studies support that osteoblast lineage cells interact with tumor cells, the exact state of differentiation of these cells remains to be defined. The Col-GFP mouse model marks osteoblasts with GFP expression throughout the stages of differentiation, and it is therefore not possible to define at which stage osteoblasts are interacting with tumor cells. All stages are likely to be increased in areas where mature osteoblasts are abundant.

To test the hypothesis that osteoblast lineage cells are directly involved in the distribution pattern of homed prostate cancer cells, AMD3100 was used to disrupt the binding of CXCL12 on osteoblasts to its receptor CXCR4 expressed by prostate cancer cells and to mobilize these cancer cells from their homing niches. This is consistent with a previous study.[5] After 5 days of treatment with AMD3100, the pattern of predominant homing of prostate cancer cells to lateral bone surfaces had disappeared. At the same time, tumor cell mobilization from the niche was suggested by an increase in the distance to the nearest bone surface following treatment with AMD3100 compared to control. As osteoblasts are proposed to be a major source of CXCL12 in the bone marrow and serve as docking sites for HSCs and prostate cancer cells,[5,10,33,34] this finding is at least partially supported in our study, which suggests that the spatial distribution of prostate cancer cells in bone marrow correlates with the location of the osteoblastic niche.

Our data suggested that AMD3100 treatment did not significantly decrease the number of prostate cancer cells in bone, but it altered the distribution of cancer cells such that they were further away from bone surfaces ($\geq$50 μm). This observation differs from a previous study, in which Shiozawa et al.[5] reported that the same AMD3100 treatment regimen mobilized prostate cancer cells from bone niches back into circulation 24 hours after treatment. This discrepancy could be due to either the fact that we captured the transition toward the vasculature of mobilized prostate cancer cells or their re-entering the niche in our study, or CXCR4/CXCL12 not being the single interaction responsible for homing of prostate cancer cells. Therefore, disruption of this single interaction may only lead to partial mobilization of homed prostate cancer cells. For example, it was reported that CXCR7 is also expressed by prostate cancer cells as an alternative receptor for CXCL12,[6,19] while AMD3100 can also bind to CXCR7 as an allosteric agonist, opposite to its antagonistic nature to CXCR4.[35] In addition, other CXCL12-independent mechanisms have also been suggested to be involved in prostate cancer cells and HSCs homing niche competition process, such as annexin II (Anxa2), c-kit, and vascular cell adhesion molecule-1 (VCAM-1)/integrins α4β1 (also known as the very late antigen-4, VLA-4).[36–42] Although it is likely that the location of tumor cells to specific niches is mediated by direct interactions between cells/matrices, it is also possible that soluble growth factors expressed by osteoblasts, such as vascular endothelial growth factor (VEGF), BMPs, and insulin-like growth factors (IGFs),[43–47] play important roles in the homing process. Such factors could induce tumor-associated angiogenesis, differentiation/growth arrest, but most importantly allow migration/survival of cancer cells in osteoblast-rich environments. All these mechanisms may help the prostate cancer cells stay in close proximity to bone marrow microenvironment, even after mobilized by CXCR4 inhibitors.

Vascular and/or perivascular niches may also contribute to this spatial distribution of homed cancer cells. Metastatic foci have often been observed in regions with abundant sinusoids, which are a main form of vascular supply in bone marrow rather than capillary beds.[48] Cancer cells have been shown to be rapidly engrafted into the perivascular regions around the bone marrow sinusoidal network.[49–51] This is thought to be to the result of the high expression of adhesive proteins including E-selection, P-selection, intercellular adhesion molecule (ICAM-1), and VCAM-1 by the endothelial cells of the bone sinusoids.[48,50] Indeed, our data underline these findings and showed that there was no difference in tumor cell numbers between lateral and medial regions within 24 hours after the injection of prostate cancer cells, which suggested at earlier time points that the cancer cells are most likely still associated with blood vessels. However, there is still limited knowledge of the anatomical distribution of sinusoids in murine bone marrow. Whether or not the sinusoids are located predominately in the lateral endocortical surface is still unknown. Therefore, further investigations to quantify the anatomical distribution of sinusoids in bone marrow are needed to elucidate whether the vascular niche also correlated with the distribution of homed prostate cancer cells in later stage of

colonization. This will in turn provide evidence for whether osteoblast and vascular niche coordinates the control of the homing of prostate cancer cells in bone.

Taken together, this is the first study to provide direct evidence identifying the locations of osteoblast-rich niches to which the prostate cancer cells home in the early stage of bone metastasis. In patients, metastatic hotspots include sites with high bone turnover such as vertebral bodies and metaphysis regions of long bone.[52] Indeed, this has been highlighted by several successful clinical trials applying bone-homing radiopharmaceuticals (strontium-89, samarium, and rhenium) to sites of increased osteoblast activity.[53] While these trials are focused on targeting osteosclerotic cancer-induced bone diseases where metastatic growth is advanced, our study suggests that early targeting of areas of high bone turnover could inhibit cancer cell homing. Interestingly, early use of bisphosphonate inhibits the initiation of bone metastasis in both clinical trials and xenograft models, possibly via disruption of the interactions between osteoblasts and cancer cells.[54,55] Targeting the osteoblast abundant regions, where a higher frequency of prostate cancer cells could be expected, may be a useful strategy for preventing bone metastases. In addition, our study also underlined the therapeutic potential to use HSC niche mobilization agents (such as AMD3100) in conjunction with conventional chemotherapy to both eliminate the chemotherapy resistant dormant prostate cancer cells and target the growing metastasis at the same time.[16]

Disclosures

All authors state that they have no conflicts of interest.

Acknowledgments

This project was supported by the program grant "Defining the Bone Metastasis Niche" funded by Cancer Research UK (CRUK). PIC is funded by Mrs Gibson and the Ernest Heine Family Foundation. We also wish to thank the staff at the Bone Analysis Lab, The University of Sheffield, UK, for their excellent technical support. We also thank Clare McCartney, Jan Bilton, and Ben Woodman from St James's Biological Services, University of Leeds for their assistance.

Authors' roles: Study design: NW, TD, PC, IH, CE. Study conduct: NW, TD, KR. Data collection: NW, FD, AF, TD. Data analysis: NW, HB, CE. Data interpretation: NW, PO, PC, IH, CE. Drafting manuscript: NW and CE. Revising manuscript content: NW, HB, PO, PC, IH, CE. Approving final version of manuscript: PC, IH, CE. NW and CE take responsibility for the integrity of the data analysis.

References

1. Jemal A, Bray F, Center MM, Ferlay J, Ward E, Forman D. Global cancer statistics. CA Cancer J Clin. 2011;61(2):69–90.
2. Bubendorf L, Schopfer A, Wagner U, Sauter G, Moch H, Willi N, et al. Metastatic patterns of prostate cancer: an autopsy study of 1,589 patients. Hum Pathol. 2000;31(5):578–83.
3. Schofield R. The relationship between the spleen colony-forming cell and the haemopoietic stem cell. Blood Cells. 1978;4(1–2):7–25.
4. Paget S. The distribution of secondary growths in cancer of the breast. 1889. Cancer Metastasis Rev. 1989;8(2):98–101.
5. Shiozawa Y, Pedersen EA, Havens AM, Jung Y, Mishra A, Joseph J, et al. Human prostate cancer metastases target the hematopoietic stem cell niche to establish footholds in mouse bone marrow. J Clin Invest. 2011;121(4):1298–312.
6. Pedersen EA, Shiozawa Y, Pienta KJ, Taichman RS. The prostate cancer bone marrow niche: more than just "fertile soil." Asian J Androl. 2012;14(3):423–7.
7. Yin T, Li L. The stem cell niches in bone. J Clin Invest. 2006;116(5):1195–201.
8. Arai F, Yoshihara H, Hosokawa K, Nakamura Y, Gomei Y, Iwasaki H, et al. Niche regulation of hematopoietic stem cells in the endosteum. Ann N Y Acad Sci. 2009;1176:36–46.
9. Arai F, Hirao A, Ohmura M, Sato H, Matsuoka S, Takubo K, et al. Tie2/angiopoietin-1 signaling regulates hematopoietic stem cell quiescence in the bone marrow niche. Cell. 2004;118(2):149–61.
10. Taichman RS. Blood and bone: two tissues whose fates are intertwined to create the hematopoietic stem-cell niche. Blood. 2005;105(7):2631–9.
11. Calvi LM, Adams GB, Weibrecht KW, Weber JM, Olson DP, Knight MC, et al. Osteoblastic cells regulate the haematopoietic stem cell niche. Nature. 2003;425(6960):841–6.
12. Zhang J, Niu C, Ye L, Huang H, He X, Tong WG, et al. Identification of the haematopoietic stem cell niche and control of the niche size. Nature. 2003;425(6960):836–41.
13. Mancini SJ, Mantei N, Dumortier A, Suter U, MacDonald HR, Radtke F. Jagged1-dependent Notch signaling is dispensable for hematopoietic stem cell self-renewal and differentiation. Blood. 2005;105(6):2340–2.
14. Arai F, Hosokawa K, Toyama H, Matsumoto Y, Suda T. Role of N-cadherin in the regulation of hematopoietic stem cells in the bone marrow niche. Ann N Y Acad Sci. 2012;1266:72–7.
15. Hosokawa K, Arai F, Yoshihara H, Iwasaki H, Nakamura Y, Gomei Y, et al. Knockdown of N-cadherin suppresses the long-term engraftment of hematopoietic stem cells. Blood. 2010;116(4):554–63.
16. Shiozawa Y, Pienta KJ, Taichman RS. Hematopoietic stem cell niche is a potential therapeutic target for bone metastatic tumors. Clin Cancer Res. 2011;17(17):5553–8.
17. Taichman RS, Cooper C, Keller ET, Pienta KJ, Taichman NS, McCauley LK. Use of the stromal cell-derived factor-1/CXCR4 pathway in prostate cancer metastasis to bone. Cancer Res. 2002;62(6):1832–7.
18. Sun YX, Fang M, Wang J, Cooper CR, Pienta KJ, Taichman RS. Expression and activation of alpha v beta 3 integrins by SDF-1/CXC12 increases the aggressiveness of prostate cancer cells. Prostate. 2007;67(1):61–73.
19. Wang J, Shiozawa Y, Wang Y, Jung Y, Pienta KJ, Mehra R, et al. The role of CXCR7/RDC1 as a chemokine receptor for CXCL12/SDF-1 in prostate cancer. J Biol Chem. 2008;283(7):4283–94.
20. Sun YX, Wang J, Shelburne CE, Lopatin DE, Chinnaiyan AM, Rubin MA, et al. Expression of CXCR4 and CXCL12 (SDF-1) in human prostate cancers (PCa) in vivo. J Cell Biochem. 2003;89(3):462–73.
21. Sun YX, Schneider A, Jung Y, Wang J, Dai J, Cook K, et al. Skeletal localization and neutralization of the SDF-1(CXCL12)/CXCR4 axis blocks prostate cancer metastasis and growth in osseous sites in vivo. J Bone Miner Res. 2005;20(2):318–29.
22. Frost HM. From Wolff's law to the Utah paradigm: insights about bone physiology and its clinical applications. Anat Rec. 2001;262(4):398–419.
23. Kalajzic I, Kalajzic Z, Kaliterna M, Gronowicz G, Clark SH, Lichtler AC, et al. Use of type I collagen green fluorescent protein transgenes to identify subpopulations of cells at different stages of the osteoblast lineage. J Bone Miner Res. 2002;17(1):15–25.
24. Wang N, Robaye B, Agrawal A, Skerry TM, Boeynaems JM, Gartland A. Reduced bone turnover in mice lacking the P2Y(13) receptor of ADP. Mol Endocrinol. 2012;26(1):142–52.
25. Dempster DW, Compston JE, Drezner MK, Glorieux FH, Kanis JA, Malluche H, et al. Standardized nomenclature, symbols, and units for bone histomorphometry: a 2012 update of the report of the ASBMR Histomorphometry Nomenclature Committee. J Bone Miner Res. 2013;28(1):2–17.

26. Yumoto K, Berry JE, Taichman RS, Shiozawa Y. A novel method for monitoring tumor proliferation in vivo using fluorescent dye DiD. Cytometry A. 2014;85:548–55.
27. Reeves KJ, van der Pluijm G, Cecchini MG, Eaton CL, Hamdy FC, Brown NJ. Prostate cancer cells home to bone in a new in vivo model of bone metastasis. FASEB J. 2009;23:(927).
28. Reeves KJ, van der Pluijm G, Cecchini MG, Eaton CL, Hamdy FC, Brown NJ. Abstract 2402: Prostate cancer cell homing to bone invivo is modulated by zoledronic acid. Cancer Res. 2011;71(8 Supplement 1):2402.
29. Bragado P, Sosa MS, Keely P, Condeelis J, Aguirre-Ghiso JA. Microenvironments dictating tumor cell dormancy. Recent Results Cancer Res. 2012;195:25–39.
30. Kobayashi A, Okuda H, Xing F, Pandey PR, Watabe M, Hirota S, et al. Bone morphogenetic protein 7 in dormancy and metastasis of prostate cancer stem-like cells in bone. J Exp Med. 2011;208(13):2641–55.
31. Marlow R, Honeth G, Lombardi S, Cariati M, Hessey S, Pipili A, et al. A novel model of dormancy for bone metastatic breast cancer cells. Cancer Res. 2013;73(23):6886–99.
32. Jayakumar P, Di Silvio L. Osteoblasts in bone tissue engineering. Proc Inst Mech Eng H. 2010;224(12):1415–40.
33. Keller ET. Prostate cancer cells metastasize to the hematopoietic stem cell niche in bone. Asian J Androl. 2011;13(4):622–3.
34. Zhu J, Garrett R, Jung Y, Zhang Y, Kim N, Wang J, et al. Osteoblasts support B-lymphocyte commitment and differentiation from hematopoietic stem cells. Blood. 2007;109(9):3706–12.
35. Kalatskaya I, Berchiche YA, Gravel S, Limberg BJ, Rosenbaum JS, Heveker N. AMD3100 is a CXCR7 ligand with allosteric agonist properties. Mol Pharmacol. 2009;75(5):1240–7.
36. Jung Y, Wang J, Song J, Shiozawa Y, Havens A, Wang Z, et al. Annexin II expressed by osteoblasts and endothelial cells regulates stem cell adhesion, homing, and engraftment following transplantation. Blood. 2007;110(1):82–90.
37. Czechowicz A, Kraft D, Weissman IL, Bhattacharya D. Efficient transplantation via antibody-based clearance of hematopoietic stem cell niches. Science. 2007;318(5854):1296–9.
38. Shiozawa Y, Havens AM, Jung Y, Ziegler AM, Pedersen EA, Wang J, et al. Annexin II/annexin II receptor axis regulates adhesion, migration, homing, and growth of prostate cancer. J Cell Biochem. 2008;105(2):370–80.
39. Matsuura N, Puzon-McLaughlin W, Irie A, Morikawa Y, Kakudo K, Takada Y. Induction of experimental bone metastasis in mice by transfection of integrin alpha 4 beta 1 into tumor cells. Am J Pathol. 1996;148(1):55–61.
40. Papayannopoulou T, Priestley GV, Nakamoto B, Zafiropoulos V, Scott LM. Molecular pathways in bone marrow homing: dominant role of alpha(4)beta(1) over beta(2)-integrins and selectins. Blood. 2001;98(8):2403–11.
41. Yu C, Shiozawa Y, Taichman RS, McCauley LK, Pienta K, Keller E. Prostate cancer and parasitism of the bone hematopoietic stem cell niche. Crit Rev Eukaryot Gene Expr. 2012;22(2):131–48.
42. Schuettpelz LG, Link DC. Niche competition and cancer metastasis to bone. J Clin Invest. 2011;121(4):1253–5.
43. Roberts E, Cossigny DA, Quan GM. The role of vascular endothelial growth factor in metastatic prostate cancer to the skeleton. Prostate Cancer. 2013;2013:418340.
44. Dai J, Kitagawa Y, Zhang J, Yao Z, Mizokami A, Cheng S, et al. Vascular endothelial growth factor contributes to the prostate cancer-induced osteoblast differentiation mediated by bone morphogenetic protein. Cancer Res. 2004;64(3):994–9.
45. Spector JA, Mehrara BJ, Greenwald JA, Saadeh PB, Steinbrech DS, Bouletreau PJ, et al. Osteoblast expression of vascular endothelial growth factor is modulated by the extracellular microenvironment. Am J Physiol Cell Physiol. 2001;280(1):C72–80.
46. Phimphilai M, Zhao Z, Boules H, Roca H, Franceschi RT. BMP signaling is required for RUNX2-dependent induction of the osteoblast phenotype. J Bone Miner Res. 2006;21(4):637–46.
47. Nakasaki M, Yoshioka K, Miyamoto Y, Sasaki T, Yoshikawa H, Itoh K. IGF-I secreted by osteoblasts acts as a potent chemotactic factor for osteoblasts. Bone. 2008;43(5):869–79.
48. Bussard KM, Gay CV, Mastro AM. The bone microenvironment in metastasis; what is special about bone? Cancer Metastasis Rev. 2008;27(1):41–55.
49. Sipkins DA, Wei X, Wu JW, Runnels JM, Cote D, Means TK, et al. In vivo imaging of specialized bone marrow endothelial microdomains for tumour engraftment. Nature. 2005;435(7044):969–73.
50. Bianco P. Bone and the hematopoietic niche: a tale of two stem cells. Blood. 2011;117(20):5281–8.
51. Lehr JE, Pienta KJ. Preferential adhesion of prostate cancer cells to a human bone marrow endothelial cell line. J Natl Cancer Inst. 1998;90(2):118–23.
52. Jacobs SC. Spread of prostatic cancer to bone. Urology. 1983;21(4): 337–44.
53. Ibrahim T, Flamini E, Mercatali L, Sacanna E, Serra P, Amadori D. Pathogenesis of osteoblastic bone metastases from prostate cancer. Cancer. 2010;116(6):1406–18.
54. Miwa S, Mizokami A, Keller ET, Taichman R, Zhang J, Namiki M. The bisphosphonate YM529 inhibits osteolytic and osteoblastic changes and CXCR-4-induced invasion in prostate cancer. Cancer Res. 2005; 65(19):8818–25.
55. Saad F, Gleason DM, Murray R, Tchekmedyian S, Venner P, Lacombe L, et al. A randomized, placebo-controlled trial of zoledronic acid in patients with hormone-refractory metastatic prostate carcinoma. J Natl Cancer Inst. 2002;94(19):1458–68.